ACS Photonics

Article

pubs.acs.org/journal/apchd5

Scanning Resonator Microscopy: Integrating Whispering Gallery Mode Sensing with Atomic Force Microscopy

Sarah M. Wildgen and Robert C. Dunn*

Ralph N. Adams Institute for Bioanalytical Chemistry, University of Kansas, 2030 Becker Drive, Lawrence, Kansas 66047, United States

ABSTRACT: Scanning resonator microscopy (SRM) is developed to integrate whispering gallery mode (WGM) sensing with atomic force microscopy (AFM). The hybrid technique combines the exquisite refractive index sensing of whispering gallery mode resonators with the topography mapping capabilities of AFM. A 45 μm diameter barium titanate microsphere is attached to the end of a conventional AFM cantilever and acts as both a WGM resonator and stylus for mapping surface topography. Calibration plots, taken in contact-mode feedback, show that the WGM spectrum responds to changes in both solution and substrate refractive index. SRM imaging of a glass substrate reveals changes in surface refractive index that correspond to a small, 36 nm high feature measured simultaneously in the contact-mode topography image. Spectral measurements confirm that the contrast arises from refractive index changes and not coupling with sample topography, thus validating the approach. Additional measurements on thin polymer films and protein-coated surfaces are presented and discussed in terms of possible areas of application for SRM.

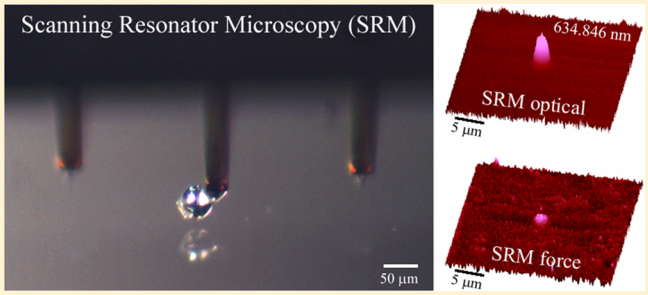

KEYWORDS: *scanning resonator microscopy, whispering gallery mode resonator, refractive index imaging, label-free sensing, surface sensing, atomic force microscopy*

Scanning probe microscopies (SPM) encompass an ever-expanding suite of techniques capable of probing surfaces with high spatial resolution.[1,2] While initially focused on mapping surface topography, significant efforts to integrate other sensing modalities into these techniques have been pursued since their introduction. This has led to an array of so-called hyphenated techniques, which have increased the capabilities and specificity of SPM measurements.

Introduced in 1986, atomic force microscopy (AFM) has proven to be a particularly flexible platform for developing hyphenated approaches.[3] Since the technique revolves around sensing mechanical forces between the tip and the sample, it affords great flexibility in sample composition and working environment. AFM measurements on samples from robust solid-state materials to soft biological tissues have been reported in environments ranging from vacuums to aqueous solutions.[4,5] Moreover, the robust and general mechanism for tip feedback can tolerate significant modifications to the tip, thus facilitating the incorporation of new sensing mechanisms. Complementary chemical, electrical, mechanical, and optical capabilities have been incorporated with AFM in order to expand analysis capabilities and increase specificity.[6,7]

The most straightforward approach for increasing the capabilities of AFM involves chemically modifying the surface of a conventional AFM tip. In chemical force microscopy (CFM), tips modified with specific functional groups have been used to probe adhesion or frictional forces between the tip and surface of interest.[8,9] More specific interactions have also been probed with tips functionalized with antibodies or other specific recognition sites.[10] Physically modifying a conventional AFM tip or replacing the tip altogether has enabled additional contrast mechanisms. For example, inspired by the success of scanning electrochemical microscopy (SECM),[11,12] microelectrodes have been integrated into AFM tips to develop scanning electrochemical-atomic force microscopy (SECM-AFM).[13−16] This enables simultaneous measurement of topography and electrochemical properties at the mesoscale. Variations of this approach have been applied to imaging redox-labeled nanoparticles and, in the life sciences, for studying enzyme activity and cellular oxidation events.[17,18]

Integrating optical contrast mechanisms with scanning probe microscopy has been a particularly active area of research given the large number of potential applications. For example, metal-coated AFM tips have been used to develop tip-enhanced Raman spectroscopy (TERS).[19] Most work in this area, however, has focused on combining fluorescence sensitivity with the high-resolution force mapping. This combination is particularly informative in biological samples, where correlations between fluorescently labeled species and surface topography can yield new structural insights. The most successful implementation is near-field scanning optical microscopy (NSOM). In apertureless NSOM, light scattered from a sharpened probe is used to excite fluorescence in the sample, while aperture NSOM uses specially fabricated fiber-

Received: December 22, 2014
Published: May 14, 2015

ACS Publications © 2015 American Chemical Society

DOI: 10.1021/ph500480x
ACS Photonics 2015, 2, 699−706

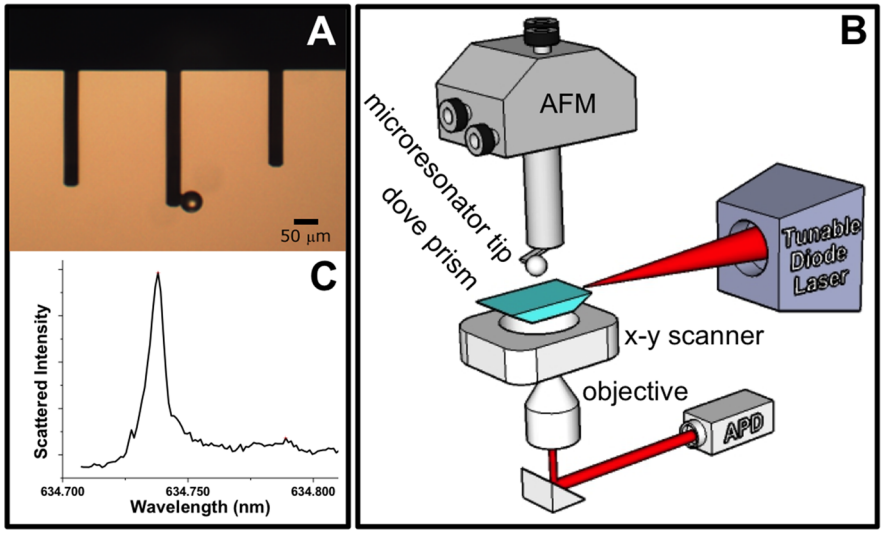

Figure 1. (A) Magnified view of an AFM cantilever with a 45 μm diameter barium titanate microsphere attached on the side. (B) Schematic of an SRM platform that combines whispering gallery mode sensing with AFM. The microresonator tip is held in an AFM head that adjusts the tip vertically in contact-mode feedback. The sample below is mounted on a Dove prism, which is held in an $x-y$ piezo scanner to scan the sample under the tip. Excitation light from a tunable diode laser is directed into the Dove prism, creating an evanescent wave at the sample surface to excite WGMs in the microresonator tip. Evanescently scattered excitation from the tip is collected from below and detected on an avalanche photodiode (APD). (C) WGM spectrum of the microresonator tip shown in (A) measured by tuning the diode laser while detecting the scattered excitation. The spectrum was collected with the tip held in contact-mode at a glass surface under aqueous conditions.

optic probes to deliver light to the nanometric dimension.[20,21] This approach provides high-resolution fluorescence and topography information with single-molecule detection limits.[22] However, for transmitted light applications where one wishes to probe optical properties such as refractive index, aperture NSOM has proven problematic. Gap-dependent coupling between the tip and sample often leads to artifacts in transmitted light images that are not easily controlled and can dominate the signal.[23] There is, however, great interest in measuring refractive index with high spatial resolution.

Refractive index probes a fundamental parameter of a material and has become increasingly important to map with high spatial resolution given recent developments in photonics and energy applications.[24−26] Refractive index is also commonly used to monitor binding events at surfaces for applications in sensing and screening.[27] Combining refractive index sensing with the high spatial resolution of AFM, therefore, can lead to new approaches for a range of applications including characterizing photonic materials and quantifying binding in high-density surface arrays. Finally, unlike fluorescence measurements, refractive index sensing does not require an intrinsic fluorophore or external tag and is not limited by photobleaching.

Combining refractive index sensitivity with AFM has been implemented using both surface plasmon resonance and ellipsometric approaches.[28−31] Ellipsometric approaches are attractive since they enable the complex refractive index to be measured, once suitable models are applied.[30] Often, however, the integration relies on combining two separate measurements onto the same microscope platform. This enables both measurements to be done in the same general area of the sample, but does not easily lead to high-resolution optical information or enable a direct pixel-by-pixel comparison between the optical and topography signals. More integrated approaches have used a conventional AFM probe to perturb an optical field at the sample interface and generate optical contrast.[31] While high-resolution contrast can be measured, this approach can suffer from coupling between optical and topographic information, which makes image analysis problematic.

Here we develop scanning resonator microscopy (SRM), which combines refractive index sensing with AFM by integrating a small optical resonator at the end of a conventional AFM probe. Small, dielectric spheres, tens of micrometers in diameter, are easily attached to AFM probes and have been used previously in force and optical measurements.[32−35] Here, we use these resonators to sense surface refractive index through changes in their whispering gallery mode resonances.

Light evanescently coupled into axially symmetric dielectric structures, such as a glass microsphere, can undergo nearly total internal reflection at each interaction with the dielectric interface.[36−43] When the light circumnavigates the microsphere and returns in phase, constructive interference leads to morphology-dependent resonances known as whispering gallery modes (WGMs). These quasi-modes are given by

$$\lambda = \frac{2\pi r n_{\text{eff}}}{m} \tag{1}$$

where λ is the wavelength of light, r is the radius of the resonator, m is an integer, and n_{eff} is the effective or orbital refractive index of the sphere. Refractive index changes, therefore, lead to shifts in the WGM resonance.[36−43]

Microsphere resonators are easily fabricated in a range of sizes and materials and, since they are formed from melts, have exceptionally smooth surfaces that lead to large quality factors (Q-factors).[36−38] High-Q resonators have long effective path lengths, as trapped light circulates within the resonator. This, combined with their narrow spectral line width ($\leq$pm), leads to sensitive refractive index detection in a compact structure, well suited for integration with AFM.

By integrating a WGM resonator at the end of a conventional AFM cantilever, we simultaneously map surface refractive index with topography. Calibration plots confirm that the WGM

DOI: 10.1021/ph500480x
ACS Photonics 2015, 2, 699−706

resonance of the tip-bound resonator responds linearly with changes in substrate refractive index. The optical resonator also acts as the stylus in contact-mode AFM, enabling surface topographical features to be directly correlated with changes in surface refractive index. Preliminary studies are carried out on a range of samples to validate the approach and demonstrate the potential of this new surface characterization technique.

RESULTS AND DISCUSSION

To integrate WGM sensing with AFM, a small microsphere resonator is attached to the end of a conventional AFM cantilever. In Figure 1A, a 45 μm diameter barium titanate microsphere (Mo-Sci Corporation) is attached to the end of an AFM cantilever using UV-curable adhesive. The AFM cantilever shown is 350 μm long and 32.5 μm wide, with a nominal spring constant of 0.03 N/m (MikroMasch, CSC38). The microsphere resonator is attached to the side of the cantilever to leave a pristine path around the sphere to support WGM resonances.

The microresonator tip is mounted in a Dimension AFM head that is incorporated into a modified Bioscope AFM (Digital Instruments), as shown schematically in Figure 1B. The AFM is built on an inverted optical microscope (Zeiss Axiovert 135) equipped with a 4× objective (Olympus PlanN, 0.10 NA). The sample is mounted below the AFM head on a Dove prism (Edmund Scientific), which is held in a closed-loop x−y piezo stage (Physik Instrumente). The x−y piezo stage raster scans the sample below the microresonator tip, while the z-piezo of the AFM head (x and y piezos disabled) adjusts the tip−sample gap in contact-mode feedback.

To excite WGM modes in the microresonator tip, light from a tunable diode laser (New Focus Vortex II TLB-7000, center wavelength 635 nm) is focused into the Dove prism.[43] Light entering the Dove prism is refracted toward the transparent sample at an angle leading to total internal reflection at the interface. The associated evanescent field at the sample surface couples radiation into the microresonator tip as it nears the surface. To measure the WGM resonance, evanescently scattered light from the resonator is collected with the microscope objective and detected on an avalanche photodiode (APD) detector (SPCM-200, EG&G). The large size of the resonator compared with the rapid decay of the evanescent field leads to scatter dominated by the lower region of the resonator, closest to the sample surface.[44−46] This results in a well-defined spot of scattered radiation from the side of the resonator that is easily collected and imaged onto the detector. The output of the APD detector is sent to a photon counting module in the AFM controller (Digital Instruments Nanoscope IIIa), which controls sample scanning and data acquisition.

Figure 1C shows the WGM spectrum of the modified microresonator AFM tip shown in Figure 1A. The WGM resonance was measured while the tip was held in contact-mode feedback at a glass surface under aqueous conditions. Spectra are measured by collecting evanescently scattered light as the wavelength of the tunable diode laser is swept.[44−46] Typical Q-factors measured for the modified microresonator AFM tips ranged from 5×10^4 to 1×10^6. The particular spectrum shown in Figure 1C, for example, indicates a measured Q-factor of 1×10^5, which is likely limited by overcoupling arising from the direct contact between the microresonator tip and sample surface.[47]

To show that the microresonator tip responds as expected, Figure 2A plots the shifts in the WGM resonance as the

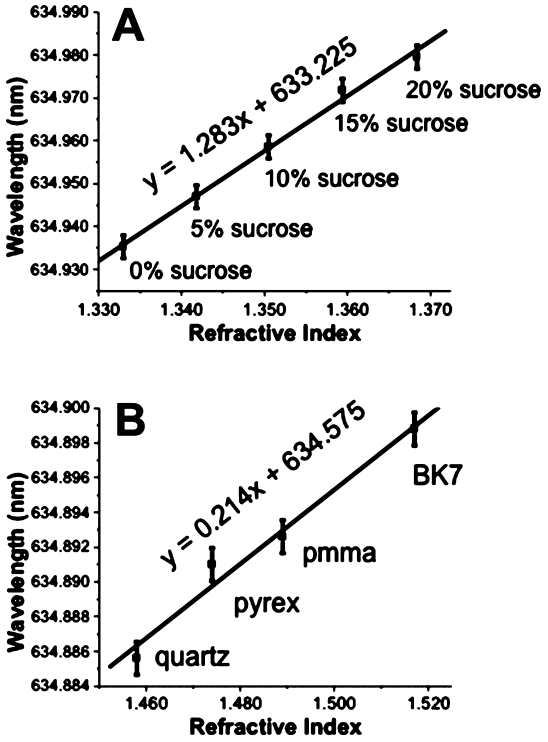

Figure 2. Refractive index calibration plots for a microresonator tip. (A) Calibration based on changes in sucrose concentration showing the expected linear trend (R^2 = 0.997) between resonant wavelength and solution refractive index with a measured detection limit of ~3.7×10^{-3} RIU. (B) Same microresonator tip calibrated using changes in substrate refractive index while holding the surrounding refractive index constant (nanopure water). A linear trend (R^2 = 0.987) is observed albeit with a decrease sensitivity, resulting in a detection limit of ~1.5×10^{-2} RIU. Error bars represent intra-assay variability (N = 3).

refractive index of the surrounding solution was systematically increased with sucrose concentration (degrees Brix). A linear red shift (R^2 = 0.997) in WGM resonant wavelength with refractive index is observed in accordance with eq 1, resulting in a detection limit of ~3.7×10^{-3} solution RIU. However, since SRM is a surface technique, calibrating the refractive index response through changes in the surrounding solution does not accurately mimic the experimental measurable. Figure 2B, therefore, shows a second calibration plot using the same microresonator tip, calibrated using changes in the substrate refractive index. In these measurements, the surrounding bath refractive index was held constant (nanopure water) while the surface refractive index was varied by changing the substrate. Figure 2B shows the linear response (R^2 = 0.987) of the resonator to surface refractive index, albeit with reduced sensitivity and a higher detection limit of ~1.5×10^{-2} substrate RIU due to the limited region of interaction between the resonator and the surface.

Having demonstrated that a microresonator tip responds to surface refractive index, Figure 3 shows initial SRM imaging measurements. For these measurements, the microsphere resonator acts as both the stylus to sense sample topography in contact-mode feedback and WGM resonator that responds to changes in surface refractive index. Figure 3A and B show 15 μm × 15 μm topography and SRM optical images, respectively, of a cleaned glass microscope slide under aqueous conditions. The image in Figure 3B was measured with the excitation

DOI: 10.1021/ph500480x
ACS Photonics 2015, 2, 699−706

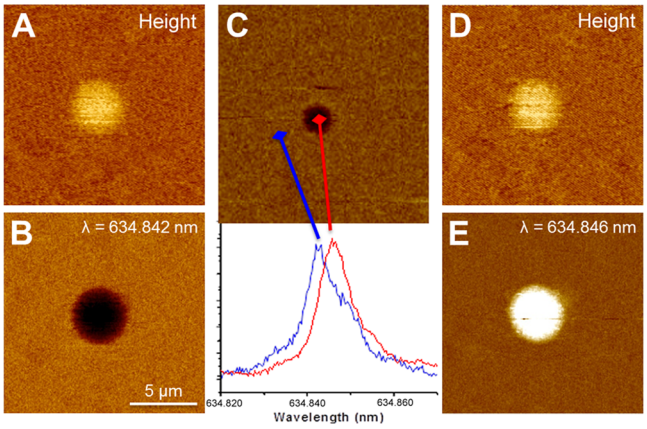

Figure 3. SRM topography (A) and optical (B) images of a cleaned glass substrate under aqueous conditions. The excitation wavelength is held constant at 634.842 nm, which corresponds to the WGM resonance of the tip on glass. The topography image reveals a small 36 nm high feature in the center of the image that corresponds to a large decrease in scattered intensity from the microresonator tip. (C) Spectra collected on and off the feature confirm the intensity decrease observed in (B) arises from a shift of the WGM resonance of the tip. SRM topography (D) and optical (E) images of the same sample region with the excitation now held at 634.846 nm, which corresponds to the WGM resonance of the tip on the feature. An increase in intensity is observed as the tip comes into resonance while scanning across the feature.

wavelength held constant at 634.842 nm, corresponding to the WGM resonance of the microresonator tip on the glass surface. The topography image reveals a small 36 nm high feature in the middle of the image due to contamination on the otherwise smooth glass surface. This feature corresponds to a large change in intensity observed in the corresponding WGM image. A large, reversible decrease in the evanescently scattered light from the microresonator tip is observed in Figure 3B as the microresonator tip scans across the feature. To confirm that the WGM contrast seen in Figure 3 arises from spectral shifts and not coupling with the surface topography, the microresonator tip was positioned and held at the locations indicated in Figure 3C while spectra were recorded. With the tip positioned 10 μm on either side of the feature, the WGM spectrum indicates a resonant wavelength at 634.842 nm. When the tip is centered on the feature, the WGM spectrum red shifts to 634.846 nm, indicating a larger refractive index than the surrounding glass substrate. These measurements confirm that the intensity contrast measured in Figure 3B arises from variations in sample refractive index and not coupling between the topography and optical signals. This is further confirmed in Figure 3D and E, where the same sample area is imaged again but with the excitation wavelength tuned to match the WGM resonance of the tip on the feature at 634.846 nm. An increase in evanescent scattering from the tip is now observed at the center of the image as the microresonator tip comes into resonance when it crosses the sample feature.

The measurements in Figure 3 illustrate the surface refractive index sensing capabilities of SRM, which should be particularly useful for characterizing thin polymer films. Thin polymer films are rapidly emerging as important materials for photonic applications where refractive index structures can be engineered into the films.[24−26] Figure 4 shows an SRM measurement on a thin film of the photoreactive polymer AZ 1518. This photoresist is used extensively in microfabrication applications

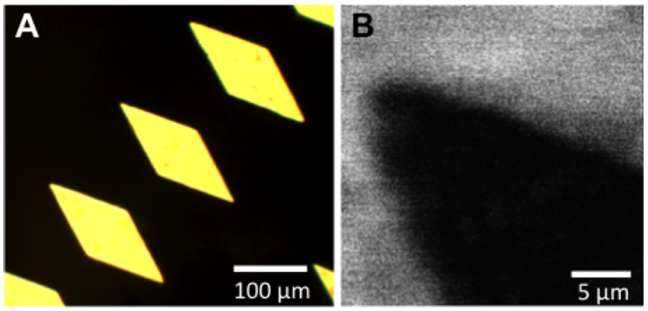

Figure 4. (A) Photolithography mask used to pattern thin films of the photoresist AZ 1518 with UV radiation. (B) SRM optical image of a thin polymer film following UV exposure. Scattered intensity decreases in UV-exposed regions of the film as the WGM resonance of the microresonator tip shifts due to refractive index changes. Images were collected in air at room temperature.

where thin films are easily fabricated on substrates by spin-casting.[48] AZ 1518 has a refractive index of 1.623 (632.8 nm), which shifts to lower values upon exposure to UV radiation as diazonaphthoquinone (DNQ) in the polymer undergoes a series of physicochemical changes that ultimately converts it to a carboxylic acid.[49−51] The final refractive index change in the exposed film depends on the degree of photoactivation and the amount of residual solvent remaining in the film following postexposure baking.[52]

To create refractive index test samples, standard photolithography techniques were used to expose thin films of AZ 1518 to UV radiation through the mask shown in Figure 4A. Following exposure, the films were baked to remove residual solvent but not processed further, leaving smooth polymer films with refractive index features encoded by the mask. Figure 4B shows a representative refractive index image of the thin film taken with SRM. The particular 45 μm diameter resonator tip used had a Q of 1×10^5, and images were collected while holding the excitation wavelength constant at 634.848 nm, corresponding to the tip resonance in contact with the unexposed regions of the polymer. In Figure 4B, a reversible shift in contrast is observed as the microresonator tip scans across the exposed regions of the polymer film, accurately mapping the exposed mask feature. The lower intensity reflects reduced scattering from the microresonator tip as the change in refractive index shifts its WGM resonance. It is important to note that these films were imaged following exposure to UV light without any further development in order to visualize the structures.

To gain a more quantitative view of the refractive index differences between the exposed and unexposed regions of AZ 1518 films, spectra were collected in both regions and the resonator was calibrated. The calibration plot shown in Figure 5 was used to calculate the refractive index values for both exposed and unexposed regions of the polymer film based on the measured WGM resonant wavelength of the tip in these regions (inset Figure 5). From Figure 5, the measured refractive index in unexposed regions is 1.610. This is lower than literature values of 1.623.[50] This difference may reflect residual solvent in the films or unintended exposure of these regions, both of which will lower the film refractive index.[52] In exposed regions of the polymer, the measured refractive index is 1.600, reflecting the expected shift to lower refractive index following UV exposure.

DOI: 10.1021/ph500480x
ACS Photonics 2015, 2, 699−706

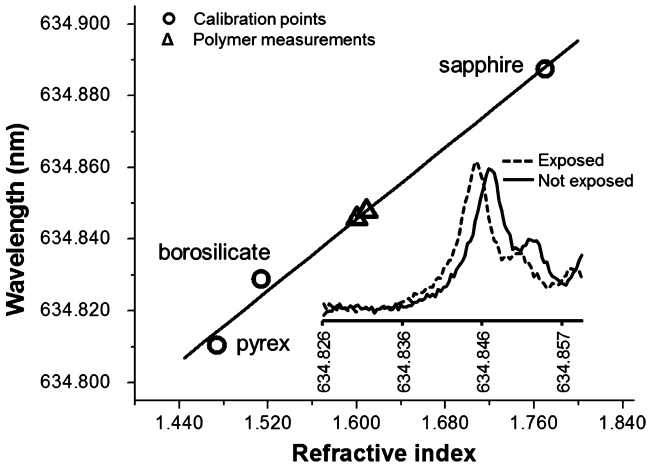

Figure 5. Calibration (circles) of the microresonator tip used in Figure 4 to quantify the changes in refractive index between exposed and unexposed regions of the polymer film (triangles). From this, the measured refractive index of exposed regions is 1.600 and that of areas not exposed is 1.610. Spectra were collected in air at room temperature.

To further explore the imaging capabilities of SRM, thin films of Teflon AF were investigated. Teflon AF is a class of transparent amorphous fluoropolymers popular in optics and electronic applications due to their low refractive index (n = 1.29), high thermal stability, and robust chemical resistance.[53,54] A 1% solution of AF2400 resin in fluorinated solvent FC40 was spin-cast onto a glass substrate to produce a thin film. The films were baked at 70 °C for 15 min to remove residual solvent and imaged dry at room temperature. Figure 6 shows typical SRM optical and topography images of a Teflon AF thin film on glass.

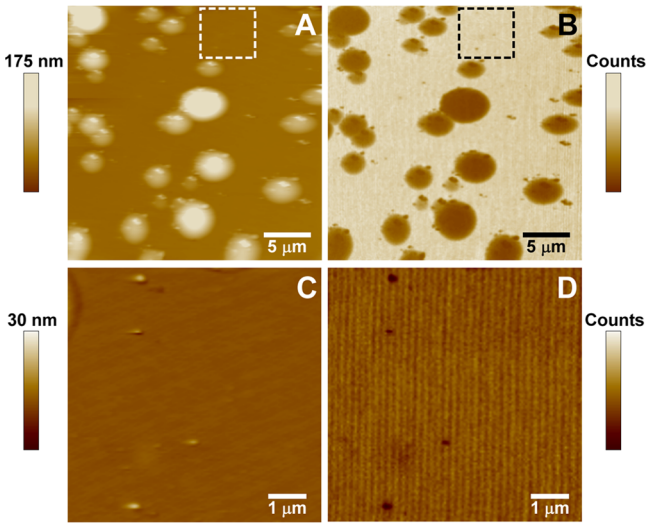

Figure 6. Simultaneously measured 28 μm × 28 μm SRM topography (A) and optical (B) images of a thin Teflon AF film in air at room temperature. Three contrast levels are observed in the SRM optical image, with the darkest features (largest WGM shift) corresponding to small particles observed alone and within the larger domains. The 8 μm × 8 μm SRM topography (C) and optical (D) images are extracted from the boxed areas in A and B. Large contrast in the SRM optical signal corresponds to small domains ranging in height from 3 to 30 nm.

The topography image in Figure 6A reveals semicircular domains approximately 50−150 nm high. Formation of the domains and film morphology strongly depends on the resin−substrate affinity as well as the substrate surface properties.[54] The corresponding SRM optical image (Figure 6B) shows decreased scattering from these features. Close inspection, however, reveals much darker contrast arising from small particles with heights ranging from 3 to 30 nm. These particles are observed decorating the larger domains and isolated in the smooth regions between domains. These particles correspond to large decreases in intensity in the SRM optical contrast even though their height is modest. This is most clearly seen in the expanded regions shown in Figure 6C and D. The measured particle height of 9 nm is near the expected globule size of the polymer particles (6 nm), and the large contrast observed in the SRM optical image is consistent with the low refractive index of the AF2400 polymer.[54]

The smallest measured lateral feature size in the SRM topography and optical images is approximately 300 nm. This provides a reasonable estimate of the SRM resolution using a 45 μm diameter resonator, given the anticipated size of the globular particles (6 nm) is much smaller than the SRM probe.[54] The resonator attached tip will also impart more force to the sample than conventional AFM probes. However, in all samples studied, no evidence of sample perturbation was observed with repeated scanning.

Finally, preliminary experiments have begun to explore the usefulness of SRM for characterizing binding at surfaces. Figure 7, for example, compares WGM spectra taken with SRM in

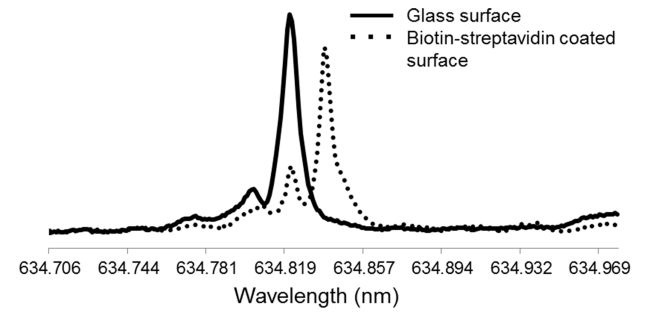

Figure 7. Example of reversible shifts in the WGM resonance of a microresonator tip held in contact-mode feedback on a bare glass surface versus a biotin−streptavidin-coated surface. Measurements were taken in PBS at room temperature.

phosphate-buffered saline (PBS) on a bare glass substrate compared with that taken on a glass surface coated with protein. For the protein surface, bovine serum albumin−biotin was covalently attached to a glass slide, which was then incubated with streptavidin in PBS. Red shifts in the measured WGM resonance are observed on the protein-coated surface, consistent with the presence of the biotin−streptavidin complex. The reversibility of the shift was confirmed by repeating the spectral measurement of the resonator on the bare glass substrate. WGM resonators are routinely used in label-free sensing applications, and the results shown in Figure 7 suggest that similar approaches can now be used to monitor binding at surfaces.[36−43] Advantages of this include the ability to use the same resonator to monitor binding of multiple analytes at various sites, thus alleviating issues in calibration and varying resonator Q-factors. This also introduces a quantitative

DOI: 10.1021/ph500480x
ACS Photonics 2015, 2, 699−706

approach for monitoring binding at high-density surface arrays that does not require the introduction of labels.

CONCLUSION

Whispering gallery mode sensing is combined with AFM to simultaneously characterize refractive index and surface topography. The preliminary data shown validate the SRM method and illustrate the flexibility of the approach for characterizing refractive index structures at surfaces. The ability to map these changes with high spatial resolution provides a new tool for material characterization and in the biological sciences. Refractive index measurements are also routinely used in sensing applications where binding events are quantified.[27,41−43] SRM enables similar measurements at surfaces. Since this approach does not require resonator functionalization, the same microresonator tip can be used to quantify binding at several sites. This approach, therefore, will simplify calibration, reduce complications arising from Q variation among resonators, and dovetail nicely with progress being made in fabricating high-density arrays.

Going forward, straightforward modifications can easily increase the performance metrics of SRM. The refractive index sensing in SRM is far from optimized, with literature WGM applications reporting 10^{-7} RIU sensitivity.[38] Coupling microspheres with tipless AFM cantilevers, moreover, will enable smaller resonators to be attached, thus increasing spatial resolution. Losses in the resonator cavity eventually limit the ultimate diameter possible, but resonators micrometers in diameter can still support WGMs.[55,56] Integrating an evanescent coupler that rides with the resonator tip will enable measurements on opaque samples and samples with large topography changes. This would also completely decouple the topography and optical signals and enable the coupler/resonator gap to be tuned toward the critical coupling condition, where resonator Q is maximized.[47] These additions will increase the sensitivity and flexibility of the SRM approach, which opens new capabilities for characterizing surfaces.

METHODS

SRM Imaging and Spectral Measurements. Barium titanate microresonators (45 μm diameter, Mo-Sci Corporation) were attached to the sides of conventional AFM cantilevers (MikroMasch CSC38) using UV-curable adhesive (Loctite 3525). The modified microresonator tip is held in a Dimension AFM head (Digital Instruments) that uses laser light (543 nm) reflected from the end of the tip to generate the feedback signal. The sample is mounted below the tip on a Dove prism, which is held in an $x-y$ closed-loop piezo scanner (Physik Instrumente) that raster scans the sample. Both AFM head and sample scanner are mounted on an inverted optical microscope (Zeiss Axiovert 135) using a design similar to the Bioscope AFM (Digital Instruments).

WGM excitation from a tunable diode laser centered at 635 nm (New Focus Vortex II TLB-7000) is focused into the Dove prism, which refracts the light to the sample interface at an angle leading to total internal reflection. The evanescent field at the sample surface can couple light into the microresonator as the modified AFM tip is lowered into the field. To measure tip WGM resonances, the wavelength of the laser is scanned as evanescently scattered excitation from the tip is collected from below with the inverted microscope (Olympus Plan N 4×, 0.10 NA) and detected on an avalanche photodiode detector (SPCM-200, EG&G). Laser control, sample scanning, tip feedback, and signal collection are all integrated with a modified AFM controller and software (Digital Instruments Nanoscope IIIa).

All measurements are done with the microresonator tip held at the sample surface in contact-mode feedback. For SRM imaging, the diode laser is tuned to the WGM resonance of the tip and held at that wavelength during imaging. To calibrate the response of each tip, the substrate (ESCO Optics) refractive index was varied as indicated. All calibrations were done without sample scanning while holding the tip in feedback mode on the surface. All spectral measurements and imaging were carried out at room temperature and under aqueous or dry conditions as specified.

Thin Films. Thin films of AZ 1518, a photoreactive polymer, and Teflon AF, a fluorinated polymer, were created and analyzed using SRM. To prepare AZ 1518 polymer thin films, unmodified AZ 1518 (AZ Electronic Materials) was spin-cast (Brewer Science Cee 100) onto clean microscope slides (Fisherbrand cover glass) to a thickness of 1−2 μm, as verified using surface profilometry (Tencor Alpha-step 200). Custom photolithography masks were designed in AutoCAD and fabricated by Infinite Graphics, Inc. Films were soft baked (2 min at 100 °C), aligned with the mask, and then exposed to 365 nm radiation (ABM Mask Aligner, i-line flood source) to modify the polymer structure. Exposure times varied from 15 to 30 s. Following exposure, samples were hard baked (10 min at 100 °C) to remove residual solvent and increase the refractive index contrast. SRM measurements were carried out in air using contact-mode feedback at room temperature.

To prepare Teflon AF (DuPont) thin films, 1 μL of a 1% solution of AF2400 in fluorinated solvent FC40 (3M) was spin-cast onto clean microscope slides. Films were baked (15 min at 70 °C) to remove most of the solvent. No further baking steps were taken in order to enhance optical and height contrast of the thin film for imaging. SRM measurements were carried out in air using contact-mode feedback at room temperature.

Protein-Coated Slides. Microscope slides were cleaned in pirhana solution (70:30 H_2SO_4/H_2O_2) and subsequently rinsed with deionized water, ethanol, and toluene. *Pirhana solution is extremely dangerous and should only be used in a properly vented hood using appropriate attire and precautions.* The clean slides were reacted in 5% (3-aminopropyl)triethoxysilane (APTES)/toluene for approximately 2 h and rinsed in toluene, ethanol, and finally PBS. The functionalized slides were incubated in 5% gluteraldehyde in PBS for 1 h. Aldehydes on the surface were reacted with bovine serum albumin (BSA)−biotin (Thermo Scientific), which was then incubated with streptavidin (Thermo Scientific). SRM experiments comparing bare glass slides with protein-coated surfaces were carried out in PBS at room temperature. All reagents were purchased from Fisher Scientific unless otherwise noted.

AUTHOR INFORMATION

Corresponding Author

*E-mail: rdunn@ku.edu.

Notes

The authors declare no competing financial interest.

ACKNOWLEDGMENTS

S.M.W. gratefully acknowledges support from the Madison and Lila Self Foundation. The authors thankfully acknowledge

DOI: 10.1021/ph500480x
ACS Photonics 2015, 2, 699−706

support from NSF (CBET 1133814). Photolithography samples were prepared at the Ralph N. Adams Institute COBRE Core Microfabrication Facility (P20 GM103638).

REFERENCES

(1) Cricenti, A.; Colonna, S.; Girasole, M.; Gori, P.; Ronci, F.; Longo, G.; Dinarelli, S.; Luce, M.; Rinaldi, M.; Ortenzi, M. Scanning Probe Microscopy in Material Science and Biology. *J. Phys. D: Appl. Phys.* **2011**, *44*, 1−23.
(2) Raigoza, A. F.; Dugger, J. W.; Webb, L. J. Review: Recent Advances and Current Challenges in Scanning Probe Microscopy of Biomolecular Surfaces and Interfaces. *ACS Appl. Mater. Interfaces* **2013**, *5*, 9249−9261.
(3) Binnig, G.; Quate, C. F.; Gerber, C. Atomic Force Microscope. *Phys. Rev. Lett.* **1986**, *56*, 930−933.
(4) Shao, Z.; Mou, J.; Czajkowsky, D. M.; Yang, J.; Yuan, J.-Y. Biological Atomic Force Microscopy: What is Achieved and What is Needed. *Adv. Phys.* **1996**, *45*, 1−86.
(5) Giessibl, F. J. Advances in Atomic Force Microscopy. *Rev. Mod. Phys.* **2003**, *75*, 949−983.
(6) Eifert, A.; Kranz, C. Hyphenating Atomic Force Microscopy. *Anal. Chem.* **2014**, *86*, 5190−5200.
(7) Flores, S. M.; Toca-Herrera, J. L. The New Future of Scanning Probe Microscopy: Combining Atomic Force Microscopy with Other Surface-Sensitive Techniques, Optical Microscopy and Fluorescence Techniques. *Nanoscale* **2009**, *1*, 40−49.
(8) Barattin, R.; Voyer, N. Chemical Modifications of AFM Tips for the Study of Molecular Recognition Events. *Chem. Commun.* **2008**, 1513−1532.
(9) Frisbie, C. D.; Rozsnyai, L. F.; Noy, A.; Wrighton, M. S.; Lieber, C. M. Functional Group Imaging by Chemical Force Microscopy. *Science* **1994**, *265*, 2071−2074.
(10) Palacio, M. L. B.; Schricker, S. R.; Bhushan, B. Protein Conformation Changes on Block Copolymer Surfaces Detected by Antibody-Functionalized Atomic Force Microscope Tips. *J. Biomed. Mater. Res., Part A* **2012**, *100A*, 18−25.
(11) Amemiya, S.; Bard, A. J.; Fan, F.-R. F.; Mirkin, M. V.; Unwin, P. R. Scanning Electrochemical Microscopy. *Annu. Rev. Anal. Chem.* **2008**, *1*, 95−131.
(12) Engstrom, R. C.; Pharr, C. M. Scanning Electrochemical Microscopy. *Anal. Chem.* **1989**, *61*, 1099A−1104A.
(13) Kranz, C. Recent Advancements in Nanoelectrodes and Nanopipettes Used in Combined Scanning Electrochemical Microscopy Techniques. *Analyst* **2014**, *139*, 336−352.
(14) Macpherson, J. V.; Unwin, P. R. Combined Scanning Electrochemical-Atomic Force Microscopy. *Anal. Chem.* **2000**, *72*, 276−285.
(15) Kranz, C.; Friedbacher, G.; Mizaikoff, B.; Lugstein, A.; Smoliner, J.; Bertagnolli, E. Integrating an Ultramicroelectrode in an AFM Cantilever: Combined Technology for Enhanced Information. *Anal. Chem.* **2001**, *73*, 2491−2500.
(16) Derylo, M. A.; Morton, K. C.; Baker, L. A. Parylene Insulated Probes for Scanning Electrochemical-Atomic Force Microscopy. *Langmuir* **2011**, *27*, 13925−13930.
(17) Huang, K.; Anne, A.; Bahri, M. A.; Demaille, C. Probing Individual Redox PEGylated Gold Nanoparticles by Electrochemical-Atomic Force Microscopy. *ACS Nano* **2013**, *7*, 4151−4163.
(18) Kueng, A.; Kranz, C.; Lugstein, A.; Bertagnolli, E.; Mizaikoff, B. Integrated AFM-SECM in Tapping Mode: Simultaneous Topographical and Electrochemical Imaging of Enzyme Activity. *Angew. Chem., Int. Ed.* **2003**, *42*, 3238−3240.
(19) Schmid, T.; Opilik, L.; Blum, C.; Zenobi, R. Nanoscale Chemical Imaging Using Tip-Enhanced Raman Spectroscopy: A Critical Review. *Angew. Chem., Int. Ed.* **2013**, *52*, 5940−5954.
(20) Krug, J. T., II; Sanchez, E. J.; Xie, X. S. Design of Near-Field Optical Probes with Optimal Field Enhancement by Finite Difference Time Domain Electromagnetic Simulation. *J. Chem. Phys.* **2002**, *116*, 10895−10901.
(21) Dunn, R. C. Near-Field Scanning Optical Microscopy. *Chem. Rev.* **1999**, *99*, 2891−2927.
(22) Betzig, E.; Chichester, R. J. Single Molecules Observed by Near-Field Scanning Optical Microscopy. *Science* **1993**, *262*, 1422−1425.
(23) Hecht, B.; Bielefeldt, H.; Inouye, Y.; Pohl, D. W. Facts and Artifacts in Near-Field Optical Microscopy. *J. Appl. Phys.* **1997**, *81*, 2492−2498.
(24) Ma, H.; Jen, A. K. Y.; Dalton, L. R. Polymer-Based Optical Waveguides: Materials, Processing, and Devices. *Adv. Mater.* **2002**, *14*, 1339−1365.
(25) Boehm, J.; Hausselt, J.; Henzi, P.; Litfin, K.; Hanemann, T. Tuning the Refractive Index of Polymers for Polymer Waveguides Using Nanoscaled Ceramics or Organic Dyes. *Adv. Eng. Mater.* **2004**, *6*, 52−57.
(26) Flory, F.; Escoubas, L. Optical Properties of Nanostructured Thin Films. *Prog. Quantum Electron.* **2004**, *28*, 89−112.
(27) Fan, X.; White, I. M.; Shopova, S. I.; Zhu, H.; Suter, J. D.; Sun, Y. Sensitive Optical Biosensors for Unlabeled Targets: A Review. *Anal. Chim. Acta* **2008**, *620*, 8−26.
(28) Chen, X.; Shakesheff, K. M.; Davies, M. C.; Heller, J.; Roberts, C. J.; Tendler, S. J. B.; Williams, P. M. Degradation of a Thin Polymer Film Studied by Simultaneous in Situ Atomic Force Microscopy and Surface Plasmon Resonance Analysis. *J. Phys. Chem.* **1995**, *99*, 11537−11542.
(29) Servoli, E.; Maniglio, D.; Aguilar, M. R.; Motta, A.; San Roman, J.; Belfiore, L. A.; Migliaresi, C. Quantitative Analysis of Protein Adsorption via Atomic Force Microscopy and Surface Plasmon Resonance. *Macromol. Biosci.* **2008**, *8*, 1126−1134.
(30) Karageorgiev, P.; Orendi, H.; Stiller, B.; Brehmer, L. Scanning Near-Field Ellipsometric Microscope-Imaging Ellipsometry with a Lateral Resolution in Nanometer Range. *Appl. Phys. Lett.* **2001**, *79*, 1730−1732.
(31) Tranchida, D.; Diaz, J.; Schoen, P.; Schoenherr, H.; Vancso, G. J. Scanning Near-Field Ellipsometry Microscopy: Imaging Nanomaterials with Resolution Below the Diffraction Limit. *Nanoscale* **2011**, *3*, 233−239.
(32) Butt, H.-J.; Cappella, B.; Kappl, M. Force Measurements with the Atomic Force Microscope: Technique, Interpretation and Applications. *Surf. Sci. Rep.* **2005**, *59*, 1−152.
(33) Amini, S.; Sun, Z.; Meininger, G. A.; Meissner, K. E. Using the Atomic Force Microscope as a Nanomechanical Partner to Support Evanescent Field Imaging. *Eur. Phys. J.* **2014**, 2023−2033.
(34) Ghislain, L. P.; Elings, V. B. Near-Field Scanning Solid Immersion Microscope. *Appl. Phys. Lett.* **1998**, *72*, 2779−2781.
(35) Stuart, J. K.; Hlady, V. Reflection Interference Contrast Microscopy Combined with Scanning Force Microscopy Verifies the Nature of Protein-Ligand Interaction Force Measurements. *Biophys. J.* **1999**, *76*, 500−508.
(36) Vahala, K. J. Optical Microcavities. *Nature* **2003**, *424*, 839−846.
(37) Vollmer, F.; Arnold, S. Whispering-Gallery-Mode Biosensing: Label-Free Detection Down to Single Molecules. *Nat. Methods* **2008**, *5*, 591−596.
(38) Hanumegowda, N. M.; Stica, C. J.; Patel, B. C.; White, I.; Fan, X. Refractometric Sensors Based on Microsphere Resonators. *Appl. Phys. Lett.* **2005**, *87*, 1−3.
(39) Matsko, A. B.; Ilchenko, V. S. Optical Resonators with Whispering-Gallery Modes-Part I: Basics. *IEEE J. Sel. Top. Quantum Electron.* **2006**, *12*, 3−14.
(40) Arnold, S. Microspheres, Photonic Atoms and the Physics of Nothing. *Am. Sci.* **2001**, *89*, 414−421.
(41) Vollmer, F.; Arnold, S.; Keng, D. Single Virus Detection from the Reactive Shift of a Whispering-Gallery Mode. *Proc. Natl. Acad. Sci. U.S.A.* **2008**, *105*, 20701−20704.
(42) Kindt, J. T.; Bailey, R. C. Biomolecular Analysis with Microring Resonators: Applications in Multiplexed Diagnostics and Interaction Screening. *Curr. Opin. Chem. Biol.* **2013**, *17*, 818−826.
(43) Huckabay, H. A.; Dunn, R. C. Whispering Gallery Mode Imaging for the Multiplexed Detection of Biomarkers. *Sens. Actuators, B* **2011**, *160*, 1262−1267.

DOI: 10.1021/ph500480x
ACS Photonics 2015, 2, 699−706

(44) Ganic, D.; Gan, X. S.; Gu, M. Three-Dimensional Evanescent Wave Scattering by Dielectric Particles. *Optik* **2002**, *113*, 135−141.
(45) Chew, H.; Wang, D. S.; Kerker, M. Elastic Scattering of Evanescent Electromagnetic Waves. *Appl. Opt.* **1979**, *18*, 2679−2687.
(46) Ashkin, A.; Dziedzic, J. M. Observation of Optical Resonances of Dielectric Spheres by Light Scattering. *Appl. Opt.* **1981**, *20*, 1803−1814.
(47) Yariv, A. Critical Coupling and its Control in Optical Waveguide-Ring Resonator Systems. *IEEE Photonics Technol. Lett.* **2002**, *14*, 483−485.
(48) Mendes, L. A. V.; Pinho, R. R.; Avila, L. F.; Lima, C. R. A.; Rocco, M. L. M. AZ-1518 Photoresist Analysis with Synchrotron Radiation Using High-Resolution Time-of-Flight Mass Spectrometry. *Polym. Degrad. Stab.* **2007**, *92*, 933−938.
(49) Avila, L. F.; Lima, C. R. A. Dill's Parameter Measure in Liquid Photosensitive Materials via Interferometric Method. *Eur. Polym. J.* **2007**, *43*, 2041−2045.
(50) Norwood, R. A.; Whitney, L. A. Rapid and Accurate Measurements of Photoresist Refractive Index Dispersion Using the Prism Coupling Method. *Proc. SPIE* **1996**, *2725*, 273−280.
(51) Henderson, C. L.; Willson, C. G.; Dammel, R. R.; Synowicki, R. A. Bleaching-Induced Changes in the Dispersion Curves of DNQ Photoresists. *Proc. SPIE* **1997**, *3049*, 585−595.
(52) Ficner, S.; Dammel, R. R.; Perez, Y.; Gardiner, A.; Willson, C. G. Refractive Indexes in Thick Photoresist Films as a Function of Bake Conditions and Film Exposure. *Proc. SPIE* **1997**, *3049*, 838−849.
(53) Lowry, J. H.; Mendlowitz, J. S.; Subramanian, N. S. Optical Characteristics of Teflon AF Fluoroplastic Materials. *Opt. Eng.* **1992**, *31*, 1982−1985.
(54) Gallyamov, M. O.; Vinokur, R. A.; Nikitin, L. N.; Said-Galiyev, E. E.; Khokhlov, A. R.; Yaminsky, I. V.; Schaumburg, K. High-Quality Ultrathin Polymer Films Obtained by Deposition from Supercritical Carbon Dioxide as Imaged by Atomic Force Microscopy. *Langmuir* **2002**, *18*, 6928−6934.
(55) Quan, H. Y.; Guo, Z. X. Analyses of Whispering-Gallery Modes in Small Resonators. *J. Micro/Nanolith. MEMS MOEMS* **2009**, *8*, 1−7.
(56) Guo, Z.; Quan, H.; Pau, S. Near-Field Gap Effects on Small Microcavity Whispering-Gallery Mode Resonators. *J. Phys. D: Appl. Phys.* **2006**, *39*, 5133−5136.

DOI: 10.1021/ph500480x
ACS Photonics 2015, 2, 699−706